RSC Medicinal Chemistry

ROYAL SOCIETY OF CHEMISTRY

RESEARCH ARTICLE

View Article Online
View Journal | View Issue

Cite this: *RSC Med. Chem.*, 2026, **17**, 1037

A new compound that extends the lifespan of worms, with favorable *in vitro* properties and a lack of toxicity in rodents

Heidi M. Blank[a] and Michael Polymenis*[ab]

Received 4th September 2025,
Accepted 22nd November 2025

DOI: 10.1039/d5md00780a

rsc.li/medchem

The development of geroprotectors, compounds that slow the biological aging process, is an important goal in modern medicine. These interventions hold the promise not only of extending lifespan, but more importantly, of extending healthspan—the period of life free from chronic disease. By targeting the fundamental mechanisms of aging, geroprotectors have the potential to simultaneously delay the onset and progression of multiple age-related conditions, thereby reducing the immense societal and economic burden of these illnesses. In this manuscript, we identified a new compound, MPOL_B_1, through a virtual screen targeting the proton-coupled folate transporter (PCFT). We describe the synthesis of MPOL_B_1 and two other lead compounds identified from the virtual screen. MPOL_B_1 had drug-like properties *in vitro* and a favorable safety profile in mice and rats. Most importantly, MPOL_B_1 increased the lifespan of the model organism *C. elegans* by up to 30%. Our findings suggest that MPOL_B_1 is a promising pro-longevity candidate that warrants further investigation, although its mechanism of action in animals requires additional studies.

1. Introduction

The enormous societal and economic impact of promoting human longevity motivates the search for compounds that extend the lifespan of model organisms from invertebrates, such as yeast, worms, and flies, to mammals, primarily mice. Results from those studies are cataloged in public databases.[1,2] Research programs managed by the National Institute on Aging systematically assess the impact of drugs on the lifespan of mice[3] and *C. elegans* worms.[4] These efforts contribute to the field of geroscience by identifying promising compounds that may help extend a healthy human lifespan.

Previous work in invertebrate model systems from several labs, including ours, implicated the conserved one-carbon (1C) metabolic pathways in longevity, and methionine restriction also extends longevity in many systems.[5–17] Furthermore, lower methyl tetrahydrofolate (THF) levels are a common signature of pro-longevity pathways.[18] We had reported that low-dose methotrexate, which limits the THF pools available for 1C reactions by inhibiting dihydrofolate reductase,[19] extended the lifespan of yeast and worms.[20] We further tested the generality of the idea that 1C pharmacologic interventions promote longevity. We inhibited ATIC (AICAR transformylase/inosine monophosphate cyclohydrolase) with an inhibitor previously shown to alleviate the metabolic syndrome in mice.[21] The ATIC inhibitor increased the lifespan of worms.[20] Following these observations, we found that restricting dietary folate in aged mice improved metabolic activity with no adverse effects.[20]

It is possible that as biosynthetic needs change in an individual's life – higher when young but lower when old, so does the role of folate-based metabolism in fulfilling those needs. Higher folate intake is beneficial in earlier stages of life when increased cell proliferation is necessary for proper development. Late in life, a lower folate intake may promote healthy aging. The contrasting effects of folate intake at different times in life can be explained by antagonistic pleiotropy, where traits beneficial early in life may have negative consequences later.[22] This mirrors the well-established example of the target of rapamycin (TOR) pathway, which promotes growth and proliferation but accelerates aging.[23] Similar to the TOR pathway, 1C metabolic pathways serve as a resource allocation platform, producing building blocks needed for biosynthesis. When dietary folate is restricted, metabolism shifts to a less anabolic state, which may promote longevity.[20] Additionally, 1C metabolism impacts various hallmarks of aging, including genomic stability, epigenetic regulation, and mitochondrial function.[24–27]

Most animals, including humans, cannot synthesize folate on their own. Folate and its various forms, such as

[a] *Department of Biochemistry and Biophysics, Texas A&M University, 300 Olsen Blvd, College Station, TX 77843, USA. E-mail: michael.polymenis@ag.tamu.edu*
[b] *Institute for Advancing Health Through Agriculture, 498 Olsen Blvd, College Station, TX 77840, USA*

5-methyltetrahydrofolate (the naturally occurring form that is absorbed through the intestinal mucosa), do not readily cross biological membranes. Instead, cells depend on receptors that bind folate to facilitate its entry. Dietary folate is primarily absorbed in the duodenum through the proton-coupled folate transporter (PCFT/SLC46A1).[28,29] By pharmacologically adjusting folate uptake, one could harness the potential benefits of reduced 1C metabolism late in life without compromising its essential role in early development. Targeting the PCFT transporter may therefore represent a novel pro-longevity approach. Here, we present our results with a new compound identified from a virtual screen to bind PCFT. We describe its synthesis, its favorable, drug-like properties, and its ability to increase the lifespan of worms. This compound's effect was 2- to 3-fold greater than the lifespan extension by methotrexate we previously published,[20] making it a promising pro-longevity candidate for further testing in mammals.

2. Results

2.1 Virtual screening for compounds that may bind PCFT

Since the high-resolution structure of PCFT/SLC46A1 has been determined (PDB: 7BC7) without and with an antifolate (pemetrexed),[30] we performed a virtual screen through molecular docking to identify compounds that may bind PCFT, using the AutoDock 4 suite.[31] The compound libraries included natural products and their derivatives (SuperNatural 3.0 (ref. 32)). Several preparatory steps were taken to ensure the PCFT target molecule and the ligands in the library were in the appropriate format for the docking algorithm to perform efficiently and accurately, as described in the Materials and methods.

The candidate compounds identified by the computational docking algorithm were first ranked based on their 'docking score', a measure of the predicted binding energy between a ligand and PCFT – the more negative the docking score value, the more favorable the predicted binding affinity. The values of the 1000 compounds with the lowest docking scores ranged between −15.4 and −11.8. Each one of these candidates was then evaluated with the SwissADME platform,[33] to gauge their potential drug-likeness. They were classified based on their molecular weight, complexity, alerts as lead, and predicted toxicity. We also further confined this set to unpatented compounds. A total of 19 compounds passed the above criteria (MW < 500, no drug-likeness violations, low complexity, predicted to be non-toxic), and they are described in the US20250002492A1 patent application filed by Texas A&M University. In the following sections of this manuscript we will describe the synthesis of three of these compounds (Table 1; PubChem compound identifiers (CIDs): 3723186, 74508575, 74577661) and experiments further focusing on one of them (CID: 3723186). We note that classic antifolates known to inhibit PCFT, such as pemetrexed, have a pyrrolo[2,3-*d*]pyrimidine core that mimics the pteridine ring system found in natural

Table 1 Three compounds identified by the computational docking screen

Compound CID	SMILES	Docking score	MW	Complexity	Synthetic accessibility	2D structure
3723186	CC(═O)N1CCC(CC1)C(═O)N2CCN3C(C2)C(═O)Nc4ccc(cc4C3═O)c5ccccc5	−12	460.5	818	3.92	
74508575	Cc1ccc(NC(═O)N2Cc3nc[nH]c3CC2c4onc(n4)c5ccc6OCOc6c5)cc1	−11.9	444.4	706	4.21	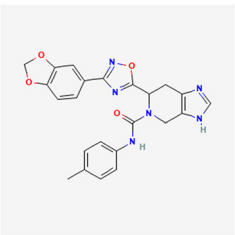
74577661	Cc1cccc(c1)c2noc(n2)C3Cc4[nH]cnc4CN3C(═O)Nc5cccc(F)c5	−11.8	418.4	641	4.11	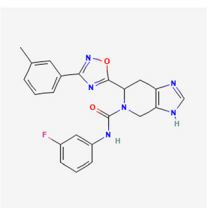

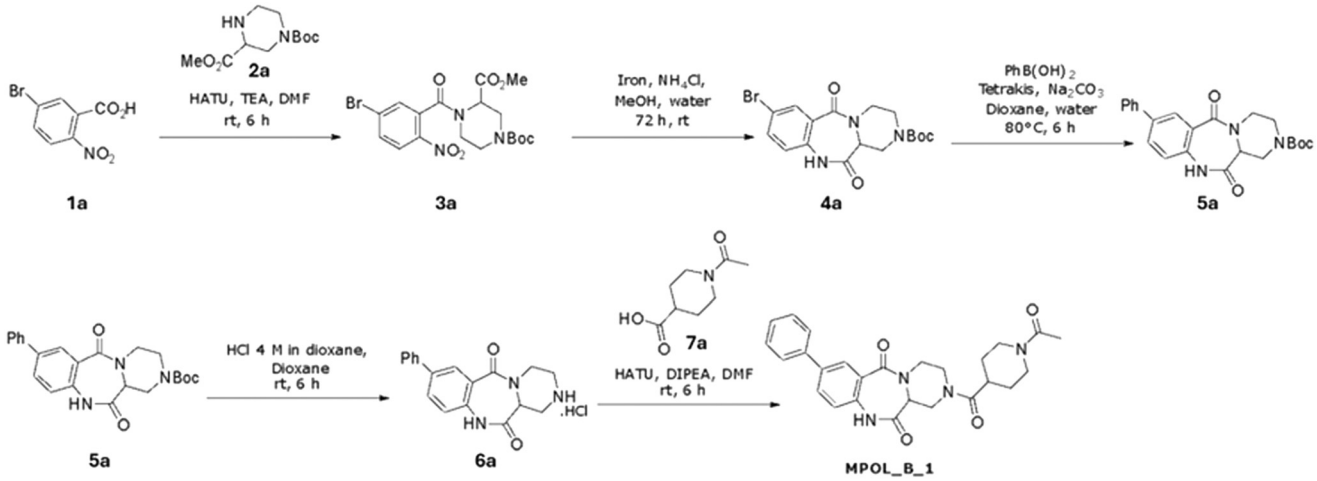

Scheme 1 Reagents and conditions for the synthesis of MPOL_B_1.

folates. Instead, the three compounds shown in Table 1 have different scaffolds. The compound with CID 3723186 has a rigid tricyclic core, giving it a significantly bulkier lipophilic profile than pemetrexed. The structural core of the other two compounds, an imidazopyridine ring system, is also distinct from the pteridine system of folic acid, albeit it is part of a broader class of heterocycles that could be developed as antifolates.

2.2 Synthesis of candidate compounds

The three compounds that we synthesized were chosen because among the other 19 candidates they had low predicted values of 'complexity' and 'synthetic accessibility', based on the SwissADME platform.[33] To simplify the naming, the compounds with CIDs 3723186, 74508575, 74577661 are referred as MPOL_B_1, MPOL_D_1, and MPOL_D_2, respectively, in this manuscript and in the US20250002492A1 patent application filed by Texas A&M University.

The synthesis of MPOL_B_1 (13-(1-acetylpiperidine-4-carbonyl)-5-phenyl-1,9,13-triazatricyclo[9.4.0.03,8]pentadeca-3(8),4,6-triene-2,10-dione) is shown in Scheme 1. First, an amide coupling reaction between compound **1a** and compound **2a**, using HATU and triethylamine, produced compound **3a** (53% yield). Then, a reduction of the nitro group of compound **3a** using iron powder and ammonium chloride produced compound **4a**, with a high yield of 93%. Compound **4a** then underwent a Suzuki–Miyaura coupling reaction with phenylboronic acid, catalyzed by tetrakis(triphenylphosphine)palladium(0), yielding compound **5a** in 67% yield. Next, a deprotection step using HCl in 1,4-dioxane quantitatively yielded compound **6a**. The final product, MPOL_B_1, was obtained through a final HATU-mediated amide coupling between compound **6a** and compound **7a**. After purification by preparative HPLC, the yield was 10%.

A convergent synthetic scheme was developed to prepare the two imidazo[4,5-*c*]pyridine derivatives, MPOL_D_1 and

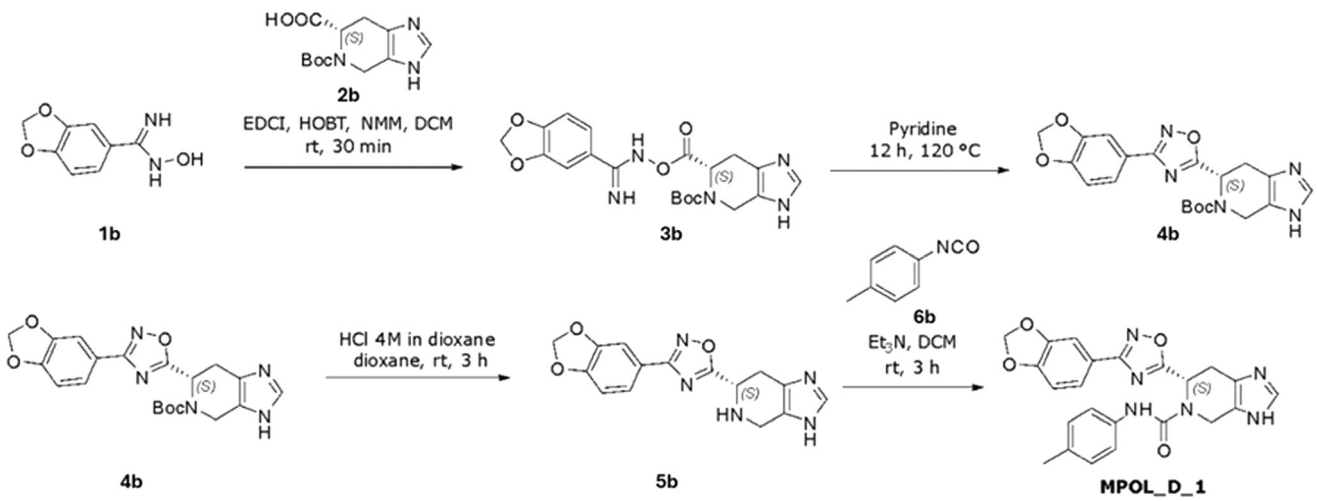

Scheme 2 Reagents and conditions for the synthesis of MPOL_D_1.

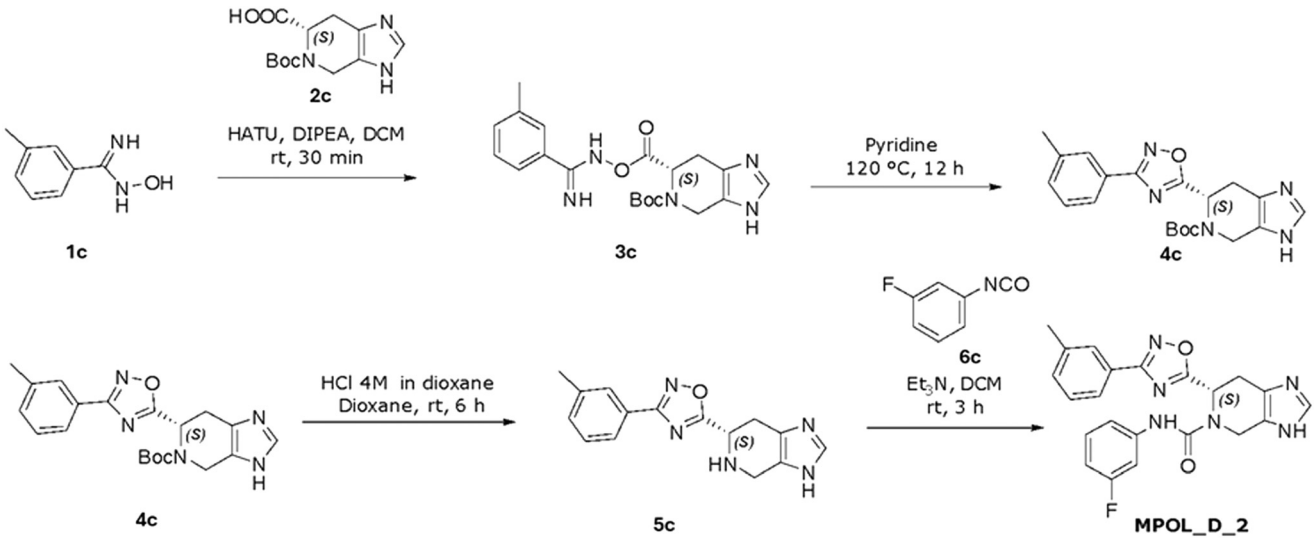

Scheme 3 Reagents and conditions for the synthesis of MPOL_D_2.

MPOL_D_2, from common intermediates. Synthesis of MPOL_D_1 (Scheme 2) began with a carbodiimide-mediated amide coupling between **1b** and **2b** using EDCI and HOBt to yield intermediate **3b** in a 37% yield. Intermediate **4b** was formed through a cyclization reaction in pyridine at 120 °C, at a 52% yield after purification by normal phase preparative chromatography. A subsequent HCl-mediated deprotection of **4b** yielded intermediate **5b** in 30% yield. The final product MPOL_D_1, (6*S*)-6-[3-(2*H*-1,3-benzodioxol-5-yl)-1,2,4-oxadiazol-5-yl]-*N*-(4-methylphenyl)3*H*,4*H*,5*H*,6*H*,7*H*-imidazo[4,5-*c*] pyridine-5-carboxamide, was made *via* a coupling reaction between **5b** and **6b**, followed by purification by reverse-phase preparative chromatography, providing the target compound as a white powder (23% yield).

To make MPOL_D_2 (Scheme 3), (6*S*)-*N*-(3-fluorophenyl)-6-[3-(3-methylphenyl)1,2,4-oxadiazol-5-yl]-3*H*,4*H*,5*H*,6*H*,7*H*-imidazo[4,5*c*]pyridine-5-carboxamide, amide coupling using HATU and DIPEA produced compound **3c** (58% yield). Cyclization formed intermediate **4c** (52% yield), which, by HCl deprotection, led to intermediate **5c** (51% yield). The final coupling and purification of MPOL_D_2 provided the target compound in 38% yield.

All final compounds were characterized by ^{1}H NMR spectroscopy, and the spectral data were consistent with their expected chemical structures (see Materials and methods, and Files S1–S4).

2.3 Testing the candidate compounds in folate transport

The three compounds were then evaluated for their ability to interfere with the transport of the sodium salt of [3,5,7,9-^{3}H] folic acid in Caco-2 cell monolayers. These cells express the PCFT transporter and under the assay conditions (pH = 5.5), folate transport is mostly PCFT dependent.[28,29] Folate uptake was quantified and normalized to total protein content for each well (see Materials and methods). The uptake rate was calculated in pmol mg^{-1} protein per min, and the inhibitory effect of each compound was expressed as a percentage of the uptake rate relative to a vehicle control (DMSO). The results from these assays are shown in Fig. 1. We conclude that MPOL_B_1 had the strongest inhibitory effect in folate uptake (42% inhibition at 50 μM) among the three new compounds we tested, albeit the effect was weaker than the known inhibitory effect of pemetrexed (62% inhibition at 50 μM).

2.4 Drug-like properties of MPOL_B_1 *in vitro*

The results of the folate transport assay led us to focus on the compound MPOL_B_1. We then experimentally evaluated its drug-like properties, which included several key variables to assess its suitability as a potential therapeutic agent. To

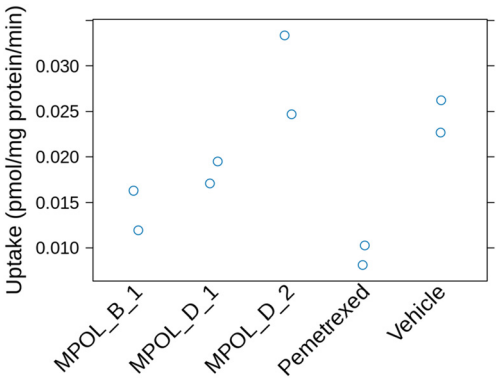

Fig. 1 Folate uptake assay in Caco-2 cells. Uptake of folate in the presence of three different compounds (MPOL_B_1, MPOL_D_1, and MPOL_D_2) was measured as described in Materials and methods. Pemetrexed, a known positive control, and a vehicle control were also included for comparison. All compounds were tested at a concentration of 50 μM. The *y*-axis is the uptake rate in picomoles per milligram of protein per minute (pmol mg^{-1} protein per min). Each data point represents an individual measurement.

Table 2 *In vitro* tests of MPOL_B_1

ASSAY	VALUE (mean ± SD)
Human plasma protein binding (2 μM)	52.5 ± 8.0 (% unbound) after 6 h
Mouse plasma protein binding (2 μM)	29.4 ± 5.9 (% unbound) after 6 h
Log *D* (octanol *vs.* PBS partitioning) (100 μM)	1.26 ± 0.02
Stability in human & mouse plasma (2 μM)	>90% after 4 h
Stability in human microsomes (2 μM)	>90% after 2 h
Stability in mouse microsomes (2 μM)	83% after 2 h
Hep2 cells cytotoxicity (50 μM)	Not significant
Caco-2 permeability (A2B) (10 μM)	P_{app} = 0.37 ± 0.04 (10^{-6} cm s^{-1})
Caco-2 permeability (B2A) (10 μM)	P_{app} = 7.17 ± 0.31 (10^{-6} cm s^{-1})
hERG K+ channel inhibition (0.1–100 μM)	IC_{50} = 86.997 μM
Ames mutagenicity test (1.4×10^{-7} to 2.3 mM)	Not mutagenic
Human liver CYP %inhibition (50 μM). The isoforms tested are shown to the right, based on co-incubation with drugs known to be metabolized by each isoform	1A2 = 5.2 ± 1.9, 2B6 = 0 ± 1.3, 2C8 = 4.9 ± 8.3, 2C9 = 11.4 ± 7.6, 2C19 = 19.4 ± 3.6, 2D6 = 16.9 ± 4.6, 3A4 = 22.5 ± 15.1

understand its behavior within a biological system, we measured its protein binding in human and mouse serum to determine how much of the drug would be free and active *versus* bound to proteins. The Log *D* value was measured as a quantitative indicator of its lipophilicity, revealing how the compound distributes between lipid and aqueous environments. We also assessed its stability in human and mouse plasma and microsomes to understand how quickly it might be broken down in the bloodstream or metabolized by liver enzymes. To evaluate its intestinal absorption, we measured its permeability using a Caco-2 cell assay, which mimics the intestinal barrier. The results from this assay also included the basolateral-to-apical (B2A) permeability ratio (P_{app}), which indicated potential efflux, where the drug is actively pumped out of the cells.

We also evaluated the potential toxicity of MPOL_B_1. We performed a cytotoxicity assay in Hep2 cells to check if the compound is harmful to these cells, an indicator of general cellular safety. The Ames test was conducted to determine if the compound has the potential to cause genetic mutations. We also performed the hERG assay to evaluate its potential to inhibit potassium channels, as hERG channel inhibition can lead to serious cardiac arrhythmias. Lastly, we assessed its ability to inhibit human liver CYP isoforms, involved in drug metabolism, to identify potential drug–drug interactions.

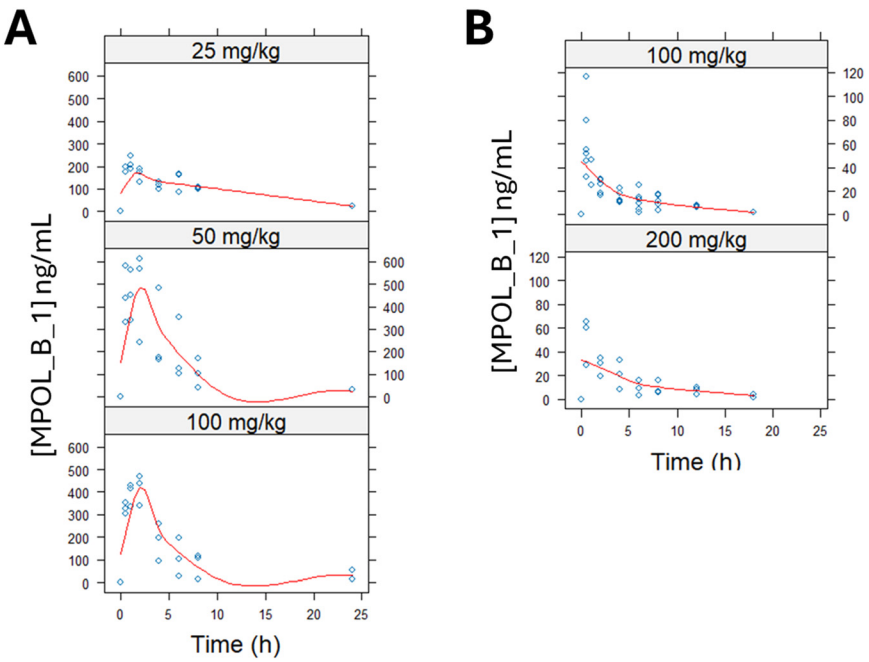

Fig. 2 Single-dose pharmacokinetics of MPOL_B_1 in mice and rats. A | Plasma concentration of MPOL_B_1 in mice. Following a single oral dose of MPOL_B_1 at 25, 50, or 100 mg kg^{-1}, plasma concentrations were measured at various time points, as described in the Materials and methods. The *y*-axis shows the concentration of MPOL_B_1 in ng mL^{-1}, while the *x*-axis is time in h. The red line represents the Loess regression fit of the data. B | Plasma concentration of MPOL_B_1 in rats. The plasma concentration-time profile of MPOL_B_1 was determined in rats after a single oral dose of 100 or 200 mg kg^{-1}, as described in the Materials and methods. The plots were drawn as in A.

The comprehensive results of these assays are summarized in Table 2, with the primary data presented in the SI figures, as referred to in the Materials and methods. Overall, the data indicate that MPOL_B_1 is safe in cell lines, is stable in biological fluids, exhibits moderate lipophilicity, shows limited potential for adverse interactions with other drugs, and has weak cell permeability with evidence of efflux. These properties suggest a favorable safety profile and potentially low systemic bioavailability, which may be beneficial for a drug designed to act primarily within the gut to target intestinal folate absorption.

2.5 MPOL_B_1 pharmacokinetics in rodents

To initiate the preclinical evaluation of MPOL_B_1, we assessed its pharmacokinetic (PK) profile and potential toxicity in single-dose studies in mice and rats. This work could inform future dose selection for repeat-dose studies. Male CD1 mice were administered MPOL_B_1 *via* oral gavage at three doses (25, 50, and 100 mg kg^{-1}). The concentration of MPOL_B_1 in serum samples was measured over 24 h by mass spectrometry (Fig. 2A). The PK profile revealed that systemic bioavailability became saturated at doses of 50 mg kg^{-1} and above, as indicated by a less-than-proportional increase in the area under the curve (AUC). For the highest dose tested (100 mg kg^{-1}), the PK parameters were: AUC_{last} = 2379 ± 1176 ng mL^{-1}, C_{max} = 416 ± 67 ng mL^{-1}, T_{max} = 1.7 ± 0.6 h, and $T_{1/2}$ = 5.7 ± 4.1 h.

Consistent with the limited systemic exposure, fecal samples collected 24 hours after administration showed high concentrations of the drug (5–10 mg g^{-1}), suggesting that the majority of the orally administered drug was not absorbed and remained within the gastrointestinal tract. This may be a beneficial characteristic for an extracellular drug designed to target intestinal folate absorption.

In male Sprague–Dawley rats, systemic bioavailability was approximately 10 times lower than in mice (Fig. 2B). We tested two doses (100 and 200 mg kg^{-1}), which yielded similar PK profiles and confirmed the low systemic absorption observed in mice. For these doses, the combined PK parameters were: AUC_{last} = 222 ± 250 ng mL^{-1}, C_{max} = 52 ± 19 ng mL^{-1}, T_{max} = 1 ± 0.9 h, and $T_{1/2}$ = 5.8 ± 2.8 h.

To assess safety, all animals in both species were monitored for 14 days following the single dose. There were no signs of illness, and no significant body weight loss was observed in any of the treated animals. At the end of the observation period, a gross necropsy was performed, revealing no organ pathologies or other abnormalities for any mice or rats that received the highest doses of MPOL_B_1. Some abnormalities were noted for some animals that received lower doses, but it is unclear that those were related to the administered compound. These results from the single-dose studies in both mice and rats support a safe profile and low systemic bioavailability for MPOL_B_1.

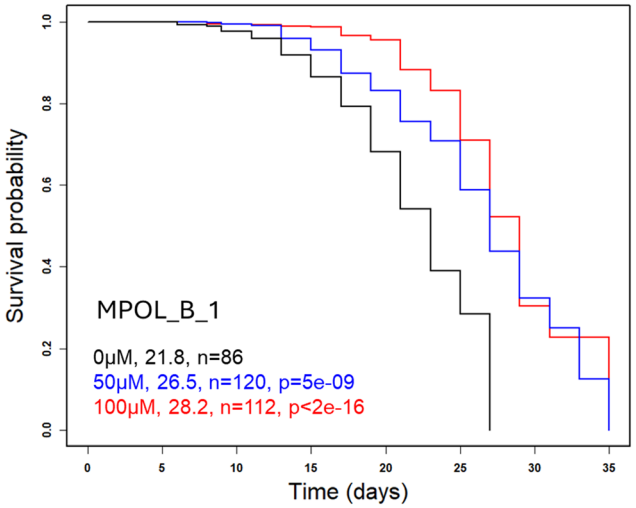

Fig. 3 Effect of MPOL_B_1 on the lifespan of *C. elegans*. The *y*-axis in the Kaplan–Meier survival curve is the survival probability. The *x*-axis indicates the time in days. Three different concentrations of MPOL_B_1 were tested: 0 μM (black line, control), 50 μM (blue line), and 100 μM (red line). The median lifespan (in days) increased from 21.8 d for untreated animals (n = 86) to 26.5 d (n = 120) and 28.2 d (n = 112) for animals exposed to 50 μM and 100 μM of MPOL_B_1, respectively. The maximal lifespan also increased from 27 d to 35 d for both treatment doses. The p-values for the log-rank test assessing lifespan extension relative to the control group are also shown.

2.6 MPOL_B_1 extends the lifespan of worms

The *in vitro* properties and pharmacokinetic profile of MPOL_B_1 in rodents suggested favorable pharmacological properties. To further test its potential, we assessed its effect on longevity using the *C. elegans* model. This genetically tractable organism provides a powerful platform for screening compounds that modulate aging.[34] Remarkably, animals continuously exposed to MPOL_B_1 had a longer maximal and mean lifespan by ~30% at 50 and 100 μM (Fig. 3). We also tested MPOL_D_1 in the same dose range (1–100 μM), but it did not exhibit similar effects (Table S4). We note that the lifespan extension by MPOL_B_1 was 2- to 3-fold greater than the extension by methotrexate, which we published using the same assay,[20] probably due to MPOL_B_1's low toxicity. These results suggest that MPOL_B_1 may hold promise as a longevity intervention, meriting further development in mammals.

3. Conclusion

Previous research, including our own, supports the idea that interventions targeting 1C metabolism may enhance longevity. Our findings with the novel compound MPOL_B_1 are encouraging, showing its potential to extend the lifespan of *C. elegans*. Additionally, the compound's safety profile observed in rodents suggests it may be a viable candidate for further development. Although the compound has low systemic availability (Fig. 2), as expected from its low permeability and high efflux ratio (Fig. S4), these properties are compatible with an intestinal site of action, where PCFT

is localized. They may also be beneficial due to lower systemic toxicity. While this work introduces a new candidate for longevity research, our data do not provide any evidence that MPOL_B_1 modulates folate uptake or folate levels in animals (including worms). Furthermore, recent work has implicated the *C. elegans* FOLR-1 folate receptor in behavioral pathways, independently of 1C metabolism. Instead, FOLR-1 regulates neuronal activity in serotonergic neurons by regulating cellular calcium levels – a role that appears to be conserved in humans.[35] Hence, the mechanisms by which MPOL_B_1 may exert its prolongevity effects remain unknown and await further experimentation. Further development of compounds that interact with PCFT would require validation of *in vivo* target engagement, after continuous oral administration, initially in mice, to evaluate their ability to modulate serum folate levels. Other experiments may also query if any healthspan metrics are improved or whether there are benefits in specific disease models. For example, selective PCFT inhibition may offer a novel strategy to harness the known anti-proliferative effects of folate reduction in rheumatoid arthritis without the systemic toxicities associated with classic antifolates like methotrexate.

4. Materials and methods

4.1 Computational docking

The virtual screen was performed by Creative Biomart Inc. (Shirley, NY), using the AutoDock 4 suite, with the following functions. First, water molecules were removed from the structure to simplify the system and make the computations fast and efficient. Second, hydrogen atoms were added to PCFT, since hydrogens not represented in the structure, especially polar ones attached to oxygen or nitrogen atoms, often participate in protein–ligand binding through hydrogen bonds. Third, the "Compute Gasteiger Charges" function was selected. This function calculates and assigns partial atomic charges to each atom in the molecule using the Gasteiger method, which were then used to calculate the electrostatic interactions between the macromolecule and the ligand. Fourth, the command "AD4 Type Assign" categorized atoms based on their chemical properties (*e.g.*, carbon, oxygen, nitrogen, *etc.*) and bonding environment (*e.g.*, aromatic carbon, aliphatic carbon), ensuring that the interaction energy calculations are accurate for a wide range of chemical groups. Lastly, to make the screening conditions more efficient, precise, and biologically relevant, they were focused on the known pemetrexed binding site of PCFT. In the AutoDock Vina module, the binding pocket was defined using the PyMol Getbox plugin to place a virtual box around the residues that form the binding site.

The ligand library was prepared as follows: first, since the ligands in the library were stored in a 2D format (SMILES), they were computationally converted to a 3D conformation from the 2D representation. Second, we used energy minimization with the MMFF94S (Merck molecular force field 94, static) type of force field to calculate the potential energy of a molecule and find the most stable, lowest-energy conformation for the ligand. Third, the optimized 3D structure was converted into a PDBQT file format, which contains all the necessary information – 3D coordinates, atom types, partial charges, and rotatable bonds, suitable for the docking software to accurately calculate the interactions and explore the conformational space of the ligand during the simulation.

4.2 Chemical synthesis

All chemical synthesis was done by Novalix Inc. (Strasbourg, France). Reagents were purchased from commercial suppliers and used without further purification. Anhydrous solvents were used as received unless otherwise stated. Reactions were monitored by thin-layer chromatography (TLC) on silica gel plates and by liquid chromatography-mass spectrometry (LC–MS). Flash column chromatography was performed on an Interchim Puriflash 430 system. Reverse-phase preparative high-performance liquid chromatography (HPLC) was performed on a C18 column using a gradient of acetonitrile and water with 0.2% ammonium bicarbonate as the mobile phase, unless noted otherwise. The certificates of analysis for each compound, along with the spectroscopic data, are provided in Files S1–S3. The detailed synthetic steps are in File S4.

4.3 Folate uptake assays in Caco-2 cells

The transport assays were done by Novalix Inc (Strasbourg, France), as detailed below.

4.3.1 Cell culture and plate preparation. Caco-2 cells were cultured in Dulbecco's modified Eagle medium (DMEM) with high glucose and L-glutamine, containing 10% fetal bovine serum (FBS), 100 U mL^{-1} penicillin, 100 μg mL^{-1} streptomycin, and 1× non-essential amino acids (NEAA). The cells were cultured in T-75 flasks at 37 °C in a humidified atmosphere of 5% CO_2, reaching 80–90% confluence before subculturing. For passaging, cells were rinsed with 5 mL of phosphate-buffered saline (PBS) and incubated for approximately 5 m in 3 mL of 0.25% trypsin and 0.53 mM EDTA solution for detachment. Trypsin was then inactivated by adding an excess of serum-containing medium. The cell suspension was centrifuged at 120*g* for 5 m, and the resulting pellet was resuspended in seeding medium. Cells were plated at a density of 3×10^4 cells per well in 24-well plates and incubated for 8–10 days. The medium was replaced every other day, beginning 48 h after plating, to allow the cells to differentiate and form a monolayer.

4.3.2 Preparation of solutions. The transport buffer was Hank's balanced salt solution (HBSS) with 10 mM MES, pH 5.5. After adding 100 mL of 10× HBSS, the pH was adjusted to 5.5 with hydrochloric acid, and the solution was filtered. Substrate and inhibitor solutions were prepared in this transport buffer. A stock solution of the sodium salt of [3,5,7,9-^{3}H] folic acid (1 mCi mL^{-1}) was diluted to a working

concentration of 10 nM. The test compounds and a positive control inhibitor, pemetrexed, were prepared at a concentration of 50 μM. For the control group, DMSO was used as the vehicle and diluted to match the final concentration in the inhibitor-containing solutions. A separate pre-incubation solution, containing either one of the test compounds, the positive control pemetrexed, or the vehicle (DMSO), was also prepared in the pH 5.5 transport buffer.

4.3.3 Uptake assay procedure. After 8–10 days of culture, the Caco-2 monolayers were used for the transport study. The medium was removed, and the cells were washed three times with 300 μL of pre-warmed pH 5.5 transport buffer. A 300 μL aliquot of the pre-incubation solution was then added to each well, and the plate was incubated at 37 °C for 30 m. The assay was performed in duplicate.

Following pre-incubation, the solution was aspirated, and 300 μL of the pre-warmed working incubation solution (containing [^{3}H]-folic acid with or without inhibitor) was added to each well to initiate the uptake assay. The incubation was carried out for 6 m, after which the reaction was stopped by rapidly washing the cells four times with 300 μL of ice-cold pH 5.5 buffer. The buffer was then removed, and 300 μL of pure water was added to each well to lyse the cells *via* three freeze–thaw cycles using liquid nitrogen and a 37 °C incubator. The cell lysates were then centrifuged at 3300*g* for 30 s. A 50 μL aliquot of the supernatant was transferred to an Isoplate-96 Microplate, mixed with 200 μL of scintillation fluid, and the radioactivity was measured for 1 m with a MicroBeta2 scintillation counter.

4.3.4 Protein quantification. Protein content was measured with a BCA (bicinchoninic acid) protein assay kit. A standard curve was based on bovine serum albumin (BSA) at concentrations ranging from 0.00391 to 2 mg mL^{-1} in PBS (pH 7.4). A 10 μL sample of the cell lysate supernatant from the uptake assay was mixed with an equal volume of PBS. A 20 μL volume of each standard or test sample was then transferred to a 96-well plate and mixed with 200 μL of the BCA working reagent. After incubating at 37 °C for 30 m, the absorbance was measured at 562 nm using a microplate reader.

4.3.5 Data analysis. The concentration of [^{3}H]-folic acid was determined from the counts per minute (CPM).

The uptake rate (pmol mg^{-1} protein per min) was calculated using the following equation: Uptake rate = Conc./(Protein × Time), where: Conc. is the concentration of drug in cell lysate (nM); Protein is the protein concentration of cell lysate (mg mL^{-1}); Time is the incubation time (m). The percentage transport (relative to the vehicle control) was calculated using the following formula: Percentage Transported (%) = R(+inhibitor)/R(vehicle control) × 100, where: R(+inhibitor) stands for the uptake rate of substrate in the presence of test compound or positive control inhibitor, and R(vehicle control) stands for the uptake rate of substrate in the vehicle control. The percentage inhibition was then determined as: Percentage Inhibition (%) = 100 − Percentage Transported (%).

4.4 *In vitro* assays for MPOL_B_1

The assays were done by Charles River Laboratories (Wilmington, MA) according to industry standards as described below. All reagents used were purchased from commercial vendors. A summary of the results are in Table 2.

4.4.1 Plasma protein binding assays. The unbound fraction of MPOL_B_1 in plasma was measured with the rapid equilibrium dialysis (RED) method, which uses a specialized 96-well plate with two chambers separated by a semipermeable membrane. One chamber was filled with either MPOL_B_1 or warfarin (positive control) at 2 μM spiked into plasma (human or mouse strain CD1), while the other was filled with a matching phosphate-buffered saline (PBS) solution at pH 7.4. The plate was sealed and incubated at 37 °C with gentle shaking for 6 h to allow the unbound drug to reach equilibrium across the membrane. After incubation, aliquots were taken from both chambers and the concentration of the compound in each aliquot was quantified using LC–MS. The results are shown in Fig. S1.

4.4.2 Log*D* assay (octanol *vs.* PBS partition) assays. To ensure equilibrium and that *n*-octanol and PBS were mutually saturated before the experiment, the two phases were vigorously mixed together and allowed to separate before use. The test compounds were prepared as stock solutions in DMSO. All compounds (MPOL_B_1, pemetrexed disodium heptahydrate, chlorpromazine – lipophilic control, warfarin – moderate control, atenolol – hydrophilic control) were tested at 100 μM. The mixture in each case was vigorously shaken for 60 m at 25 °C to allow each compound to reach equilibrium between the two phases. The samples were centrifuged to separate the organic layer (top) from the aqueous layer (bottom). The concentration of each compound in both phases was quantified using LC–MS. The ratio of each compound's concentration in the *n*-octanol phase to its concentration in the aqueous (PBS) phase was then log 10-transformed to calculate the Log*D* value, which is shown in Fig. S2.

4.4.3 Stability in plasma and microsomes. For plasma stability assays, MPOL_B_1, propantheline (used as 'stable' control), and verapamil (used as 'unstable' control) were incubated at 2 μM with human or mouse (strain CD1) plasma at 37 °C in a multi-well plate. Aliquots were taken at 0, 0.5, 1, 2, 3, and 4 h, and the reaction was immediately stopped by adding cold acetonitrile. The supernatant was collected by centrifugation, and the amounts of each compound were measured using LC–MS. The concentration of each compound at the different time points was normalized against its initial concentration (T = 0). The percentage of the parent compound remaining over time was then plotted on a logarithmic scale, as shown in Fig. S3.

Similarly, to evaluate each compound's metabolic stability and its susceptibility to cytochrome P450 (CYP) enzymes, the compounds (at 2 μM) were incubated with a suspension of liver microsomes from human or mouse (strain CD1) at 37 °C. The CYP cofactor nicotinamide adenine dinucleotide phosphate (NADPH) was added to initiate the enzymatic activity of the CYP enzymes. Aliquots were taken at the same time points as above, quenched, and analyzed by LC–MS, to yield the results shown in Fig. S3.

4.4.4 Bidirectional cell permeability assays. Caco-2 cells were cultured on 24-well Transwell plates, which feature a semipermeable membrane that separates the apical compartment (representing the intestinal lumen) from the basolateral compartment (representing the bloodstream). After approximately 21 days of culture, the cells formed a confluent, polarized monolayer with tight junctions. Using an electrode, we measured the transepithelial electrical resistance (TEER) to confirm the integrity of the monolayer. A TEER value greater than 300 Ω cm^2 indicated the presence of a tight and functional barrier. The assay was conducted in two directions to distinguish between passive diffusion and active transport.

To measure absorption (apical-to-basolateral (A→B, A2B) permeability), each compound was added to the apical (donor) chamber. The basolateral (receiver) chamber was filled with fresh buffer, and the plate was incubated at 37 °C for 2 h. Samples were then collected from the basolateral chamber at specific time points to measure the flux of the compound. To measure efflux, or active pumping out of the cells (basolateral-to-apical (B→A, B2A) permeability), the procedure was the same except that each compound was added to the basolateral chamber, while the apical chamber was filled with fresh buffer.

After incubation, the concentration of the compound in both the donor and receiver chambers was quantified using LC–MS. The apparent permeability coefficient (P_{app}, in cm s^{-1}) was calculated for each direction using the following equation: $P_{app} = C_0 \times A\Delta Q/\Delta t$, where $\Delta Q/\Delta t$ is the rate of compound transport across the monolayer, C_0 is the initial concentration of the compound in the donor chamber. A is the surface area of the cell monolayer membrane.

In addition to MPOL_B_1 (tested at 10 μM), control drugs tested in both directions were warfarin, ranitidine, talinolol (each also tested at 10 μM), and a mixture of talinolol (10 μM) plus verapamil (25 μM). The results are shown in Fig. S4.

4.4.5 P450 CYP inhibition assays. To evaluate the potential for drug–drug interactions, we performed an *in vitro* human liver microsome (HLM) cytochrome P450 (CYP) inhibition assay. The assay was designed to measure the inhibitory effect on the activity of several human CYP isoforms: CYP1A2, CYP2B6, CYP2C8, CYP2C9, CYP2C19, CYP2D6, and CYP3A4. The assay was done in 96-well plates. Each well contained a reaction mixture with HLM, the specific CYP substrate, an NADPH-regenerating system, and either MPOL_B_1 (at 10 μM) or a positive control inhibitor. The specific CYP substrates used are shown on the *y*-axis of Fig. S5. The reaction mixtures were pre-incubated at 37 °C for 30 m, and the reaction was initiated by adding the NADPH-regenerating system. After a 5 m incubation, the reaction was quenched. The samples were then centrifuged, and the supernatants analyzed by LC–MS to quantify the formation of the specific metabolite for each CYP isoform. We determined the percentage of remaining CYP activity by comparing the metabolite formation in the presence of the test compound to that of the vehicle control (100% activity). The results are shown in Fig. S5.

4.4.6 HepG2 cytotoxicity assay. The human hepatocellular carcinoma cell line HepG2 (ATCC HB-8065) was cultured in Dulbecco's modified Eagle medium (DMEM) supplemented with 10% fetal bovine serum (FBS), 100 U mL^{-1} penicillin, and 100 μg mL^{-1} streptomycin. Cells were incubated at 37 °C in a humidified atmosphere containing 5% CO_2 and were subcultured when they reached 70–80% confluence. For cytotoxicity screening, HepG2 cells were seeded into 96-well plates at ~5000 cells per well. After an overnight incubation to allow cell attachment, the test compounds were serially diluted in cell culture media to create a range of concentrations. Vehicle control wells (0.1% DMSO) and a positive control (terfenadine) were included. After the treatment period, cell viability was determined using the CellTiter-Glo® luminescent cell viability assay (Promega, WI) to quantify cellular adenosine triphosphate (ATP) as an indicator of metabolically active cells. A luminescence plate reader was used to measure the signal. The data from each well were normalized to the vehicle control to determine the percentage of cell viability for each compound concentration. The results are shown in Fig. S6.

4.4.7 hERG assay. The *in vitro* effect of MPOL_B_1 on cloned hERG potassium channels was measured on HEK293 cells expressing the KCNH2 gene. The *in vitro* effects of MPOL_B_1 were evaluated at room temperature using the QPatch II® (Sophion Bioscience A/S, Denmark), an automatic parallel patch clamp system. MPOL_B_1 was exposed to hERG at 0.1, 1, 10, and 100 μM ($n \geq 3$). The duration of exposure at each concentration was at least 6 m. Cisapride at 0.05 μM ($n \geq 2$) served as a positive control (see Table S1). Stock solutions of MPOL_B_1 and cisapride (Tocris Bioscience, Bristol, UK) were in DMSO and diluted into a HEPES-buffered physiological saline solution (HB-PS). The final concentration of DMSO in all solutions was 0.3%. Onset and block of hERG current was measured using a stimulus voltage pattern consisting of a 500 ms prepulse to −40 mV (leakage subtraction), a 2 second activating pulse to +40 mV followed by a 2 second test pulse to −40 mV. The pulse pattern was repeated continuously at 10 s intervals from a holding potential of −80 mV. Peak tail current was measured during the −40 mV test pulse. Leakage current was calculated from the current amplitude evoked by the −40 mV prepulse and subtracted from the total membrane current record. For data analysis, the steady state was defined by the limiting constant rate of change with time (linear time dependence). The steady state before and after application of each sample

was used to calculate the percentage of current inhibited at each concentration. The results are in Table S1.

4.4.8 Ames bacterial reverse mutation assays. The ability of MPOL_B_1 to induce reverse mutations was measured in *Salmonella typhimurium* tester strains TA98, TA100, TA1535, and TA1537, and in *Escherichia coli* strain WP2 uvrA, in the presence (+) and absence (−) of an exogenous metabolic activation system (phenobarbital/5,6-benzoflavone induced male rat liver homogenate with the appropriate cofactors; S9). Methods were those described in (OECD guideline 471). The negative control was DMSO, used as the vehicle for MPOL_B_1. The positive controls were sodium azide (NaAz), 9-aminoacridine hemihydrate (9AC), 2-nitrofluorene (2NF), 4-nitroquinoline *N*-oxide (NQO), 2-aminoanthracene (2AA), benzo[*a*]pyrene (BaP). MPOL_B_1 was prepared as a stock solution in DMSO (50 mg mL^{-1}), and all lower-level formulations were made directly from this stock or intermediate formulations. All formulations (and vehicle aliquot) were prepared on the day of use at ambient temperature. The bulk positive controls were also dissolved in DMSO. Toxic effects were considered positive for inducing reverse mutations if a compound induced a dose-dependent increase in revertant frequency that is at least 2-fold higher than its concurrent negative control in tester strains TA98, TA100, and WP2 uvrA, or at least 3-fold higher than its concurrent negative control in tester strains TA1535 and TA1537. If none of these criteria were met, the results were considered negative. The results without or with metabolic activation are in Tables S2 and S3, respectively.

4.5 Single-dose pharmacokinetic (PK) assays in rodents

4.5.1 Animals and study design. All animal procedures described in this study were reviewed and approved by the Institutional Animal Care and Use Committee (IACUC) of Charles River Laboratories (Worcester, MA). The specific protocols utilized were IACUC 1036 (covering procedures involving male CD1 mice) and IACUC I037 (covering procedures involving male Sprague–Dawley rats). All experiments were conducted in strict accordance with the Guide for the Care and Use of Laboratory Animals published by the National Research Council and the relevant federal, state, and institutional guidelines concerning the ethical care and use of animals. All animals, including the male CD1 mice and male Sprague–Dawley rats with pre-implanted jugular vein cannulas, received humane care and were monitored throughout the study.

Animals from both species (n = 3 per group) were sourced from an approved vendor and allowed to acclimate to the facility for at least two days before the study commenced. Mice were housed individually in metabolic cages to facilitate fecal collection and were fasted for 4 h before dosing, with food returned 2 h post-dose. Rats were also housed in metabolic cages, but they were fasted overnight, and food was returned 4 h post-dose. Water was provided *ad libitum* for both species throughout the study. Body weights for all animals were recorded prior to dose administration and on days 7 and 14. Dose volumes (10 mL kg^{-1}) were calculated based on each animal's body weight on day 1.

4.5.2 Dosing. Three dose levels of MPOL_B_1 were administered to mice and two dose levels to rats *via* oral gavage (PO). The dosing solutions were formulated in a vehicle of 40% DMSO and 60% 0.5% 400 cP methyl cellulose. Dose administration for each mouse group was: group 1: 100 mg kg^{-1} at a concentration of 10 mg mL^{-1}; group 2: 50 mg kg^{-1} at a concentration of 5 mg mL^{-1}; group 3: 25 mg kg^{-1} at a concentration of 2.5 mg mL^{-1}. Dose administration for each rat group was: group 1: 100 mg kg^{-1} at a concentration of 10 mg mL^{-1}; group 2: 200 mg kg^{-1} at a concentration of 20 mg mL^{-1}. The dose syringes were weighed before and after administration to determine the exact amount of formulation delivered to each animal.

4.5.3 Formulation preparation. Dosing solutions for all groups were prepared similarly for both mouse and rat studies. First, a 0.5% 400 cP methyl cellulose solution was prepared in distilled water. Next, stock solutions of the test article were prepared in DMSO and diluted as needed before mixing with methyl cellulose. All formulations were prepared in glass vials with stirring to minimize precipitation, and residual formulations were stored at −70 °C.

4.5.4 Sample collection. Serial blood samples were collected from both mice and rats at 0.5, 1, 2, 4, 6, 8, and 24 h post-dose. For mice, blood (~25 μL) was collected from the tail vein. For rats, blood (~200 μL) was collected from the pre-implanted jugular vein cannula. All blood was collected into K2 (dipotassium) EDTA-coated tubes and immediately placed on wet ice. Samples were processed to plasma within 30 m of collection by centrifugation at 3500 rpm for 10 m at 5 °C. Plasma was then transferred to uniquely labeled tubes and stored at −70 °C until analysis.

Fecal samples were collected over 24 h post-dose for all animals. The collection tubes, placed on ice packs, were changed at the 8 h time point. The fecal samples were transferred to pre-weighed conical tubes, and their weights were recorded. Samples were stored at −70 °C until they were transferred for analysis by LC–MS.

4.5.5 Observations and necropsy. All animals were observed at dosing and at each scheduled sample collection for any abnormalities. Following the final sample collection, all animals were humanely euthanized by carbon dioxide asphyxiation. A gross necropsy was performed on all animals to check for any abnormalities, and all gross pathological changes were recorded. No abnormalities were seen in the mouse group 1, which received the highest dose (100 mg kg^{-1}) of MPOL_B_1. One mouse in group 2 (50 mg kg^{-1}) had an enlarged stomach when gross necropsy was performed, and another from the same group had dark patches on the lungs. All three mice in group 3 that received the lowest dose (25 mg kg^{-1}) had similar dark patches on the lungs. Finally, 2 of the 6 rats in group 1, which received the lower dose of 100 mg kg^{-1}, had an

enlarged stomach and caecum and blood in the abdominal cavity at the time of necropsy.

4.5.6 Data analysis. Pharmacokinetic analysis was performed using the PKNCA R language package.

4.6 *C. elegans* lifespans

All the assays were performed at 20 °C using *C. elegans* strain N2 and a bacterial strain (OP50) commonly used as food for the worms, as described previously.[20,34] The standard OP50 bacterial strain used in nematode experiments is a strain of *Escherichia coli* (*E. coli* B) that is a uracil auxotroph. As a result of the uracil auxotrophy, OP50 grows a thin, slow-growing lawn on the nematode growth medium (NGM) plates used for culturing *C. elegans*, facilitating the movement of the animals and their observation. We note that the bacteria used to feed the worms in these experiments were killed by ultraviolet radiation to exclude any impacts from bacterial metabolism. MPOL_B_1 and MPOL_D_1 were first dissolved in DMSO and then added to the media used to prepare the plates after autoclaving (the media were kept in a 50 °C water bath until the plates were poured). Mock-treated control plates contained only DMSO. The reported lifespans were compiled from several independent experiments and analyzed with the *survival* R language package. Survival data were constructed using the Surv() function. This function defined the outcome as a survival object by specifying the time until the event of interest (death, in this case). This survival object was then used as the response variable in subsequent survival models, such as the Kaplan–Meier estimation with the survfit() function. No experiments were excluded from the analysis. The data for both drugs and all doses tested are in Table S4.

Abbreviations

1C	One-carbon metabolism
ACN	Acetonitrile
AICAR	5-Aminoimidazole-4-carboxamide ribonucleotide
ATIC	AICAR transformylase/inosine monophosphate cyclohydrolase
ATP	Adenosine triphosphate
AUC	Area under the curve
BaP	Benzo[*a*]pyrene
BCA	Bicinchoninic acid
C. elegans	*Caenorhabditis elegans*
CID	PubChem compound identifier
C_{max}	Maximum concentration
CYP	Cytochrome P450
DCM	Dichloromethane
DMEM	Dulbecco's modified Eagle medium
DMF	*N*,*N*-Dimethylformamide
DMSO	Dimethyl sulfoxide
EDCI	1-Ethyl-3-(3-dimethylaminopropyl)carbodiimide
Et_2O	Diethyl ether
Et_3N	Triethylamine
FBS	Fetal bovine serum
HATU	*N*,*N*,*N*′,*N*′-Tetramethyl-*O*-(7-azabenzotriazol-1-yl) uronium hexafluorophosphate
HB-PS	HEPES-buffered physiological saline solution
HBSS	Hank's balanced salt solution
hERG	Human *ether-à-go-go-related* gene
HLM	Human liver microsome
HOBt	1-Hydroxybenzotriazole
HPLC	High-performance liquid chromatography
IACUC	Institutional Animal Care and Use Committee
LC–MS	Liquid chromatography–mass spectrometry
MeOH	Methanol
MES	2-(*N*-Morpholino)ethanesulfonic acid
MMFF94S	Merck molecular force field 94, static
MW	Molecular weight
Na_2CO_3	Sodium carbonate
Na_2SO_4	Anhydrous sodium sulfate
NaAz	Sodium azide
NADPH	Nicotinamide adenine dinucleotide phosphate
NEAA	Non-essential amino acids
NH_4Cl	Ammonium chloride
NMR	Nuclear magnetic resonance
NQO	4-Nitroquinoline *N*-oxide
Papp	Apparent permeability coefficient
PBS	Phosphate-buffered saline
PCFT	Proton-coupled folate transporter
$Pd(PPh_3)_4$	Tetrakis(triphenylphosphine)palladium(0)
PDB	Protein Data Bank
PK	Pharmacokinetics
PO	Per oral
P-type ATPase	P-type adenosine triphosphatase
RED	Rapid equilibrium dialysis
RT	Room temperature
SD	Sprague–Dawley
SMILES	Simplified molecular-input line-entry system
TEER	Transepithelial electrical resistance
TFA	Trifluoroacetic acid
THF	Tetrahydrofolate
TLC	Thin-layer chromatography
T_{max}	Time to reach maximum concentration
TOR	Target of rapamycin
2AA	2-Aminoanthracene
2NF	2-Nitrofluorene
9AC	9-Aminoacridine hemihydrate

Author contributions

H. M. B. and M. P.: worm lifespans; M. P.: writing – original draft; H. M. B. and M. P.: writing, review and editing; M. P.: study management, funding acquisition.

Conflicts of interest

The compounds MPOL_B_1, MPOL_D_1, and MPOL_D_2 are described in the US20250002492A1 patent application filed by Texas A&M University, with M. P. listed as the lead

inventor. M. P. is the founder and manager of Krateos Therapeutics LLC.

Data availability

All relevant data are within the manuscript and its accompanying files.

Supplementary information (SI) is available. See DOI: https://doi.org/10.1039/d5md00780a.

Acknowledgements

This research was funded by a grant (M2502317) from the USDA – Agricultural Research Service and the Institute for Advancing Health Through Agriculture to M. P. M. P. was also supported by a grant from the National Institutes of Health (R01GM123139).

Notes and references

1 D. Barardo, D. Thornton, H. Thoppil, M. Walsh, S. Sharifi, S. Ferreira, A. Anžič, M. Fernandes, P. Monteiro, T. Grum, R. Cordeiro, E. A. De-Souza, A. Budovsky, N. Araujo, J. Gruber, M. Petrascheck, V. E. Fraifeld, A. Zhavoronkov, A. Moskalev and J. P. de Magalhães, The DrugAge database of aging-related drugs, *Aging Cell*, 2017, **16**, 594–597.

2 A. Moskalev, E. Chernyagina, J. P. de Magalhães, D. Barardo, H. Thoppil, M. Shaposhnikov, A. Budovsky, V. E. Fraifeld, A. Garazha, V. Tsvetkov, E. Bronovitsky, V. Bogomolov, A. Scerbacov, O. Kuryan, R. Gurinovich, L. C. Jellen, B. Kennedy, P. Mamoshina, E. Dobrovolskaya, A. Aliper, D. Kaminsky and A. Zhavoronkov, Geroprotectors.org: a new, structured and curated database of current therapeutic interventions in aging and age-related disease, *Aging*, 2015, **7**, 616–628.

3 R. A. Miller, D. E. Harrison, C. M. Astle, R. A. Floyd, K. Flurkey, K. L. Hensley, M. A. Javors, C. Leeuwenburgh, J. F. Nelson, E. Ongini, N. L. Nadon, H. R. Warner and R. Strong, An Aging Interventions Testing Program: study design and interim report, *Aging Cell*, 2007, **6**, 565–575.

4 M. Driscoll, C. A. Sedore, B. Onken, A. L. Coleman-Hulbert, E. Johnson, P. C. Phillips and G. Lithgow, NIA Caenorhabditis Intervention Testing Program: identification of robust and reproducible pharmacological interventions that promote longevity across experimentally accessible, genetically diverse populations, *GeroScience*, 2025, **47**, 2791–2816.

5 N. Maitra, C. He, H. M. Blank, M. Tsuchiya, B. Schilling, M. Kaeberlein, R. Aramayo, B. K. Kennedy and M. Polymenis, Translational control of one-carbon metabolism underpins ribosomal protein phenotypes in cell division and longevity, *eLife*, 2020, **9**, e53127.

6 C. Barcena, P. M. Quiros, S. Durand, P. Mayoral, F. Rodriguez, X. M. Caravia, G. Marino, C. Garabaya, M. T. Fernandez-Garcia, G. Kroemer, J. M. P. Freije and C. Lopez-Otin, Methionine Restriction Extends Lifespan in Progeroid Mice and Alters Lipid and Bile Acid Metabolism, *Cell Rep.*, 2018, **24**, 2392–2403.

7 F. Cabreiro, C. Au, K.-Y. Leung, N. Vergara-Irigaray, H. M. Cochemé, T. Noori, D. Weinkove, E. Schuster, N. D. E. Greene and D. Gems, Metformin retards aging in C. elegans by altering microbial folate and methionine metabolism, *Cell*, 2013, **153**, 228–239.

8 J. E. Johnson and F. B. Johnson, Methionine restriction activates the retrograde response and confers both stress tolerance and lifespan extension to yeast, mouse and human cells, *PLoS One*, 2014, **9**, e97729.

9 R. Kozieł, C. Ruckenstuhl, E. Albertini, M. Neuhaus, C. Netzberger, M. Bust, F. Madeo, R. J. Wiesner and P. Jansen-Dürr, Methionine restriction slows down senescence in human diploid fibroblasts, *Aging Cell*, 2014, **13**, 1038–1048.

10 B. C. Lee, A. Kaya and V. N. Gladyshev, Methionine restriction and life-span control, *Ann. N. Y. Acad. Sci.*, 2016, **1363**, 116–124.

11 B. C. Lee, A. Kaya, S. Ma, G. Kim, M. V. Gerashchenko, S. H. Yim, Z. Hu, L. G. Harshman and V. N. Gladyshev, Methionine restriction extends lifespan of Drosophila melanogaster under conditions of low amino-acid status, *Nat. Commun.*, 2014, **5**, 3592.

12 R. A. Miller, G. Buehner, Y. Chang, J. M. Harper, R. Sigler and M. Smith-Wheelock, Methionine-deficient diet extends mouse lifespan, slows immune and lens aging, alters glucose, T4, IGF-I and insulin levels, and increases hepatocyte MIF levels and stress resistance, *Aging Cell*, 2005, **4**, 119–125.

13 N. Orentreich, J. R. Matias, A. DeFelice and J. A. Zimmerman, Low methionine ingestion by rats extends life span, *J. Nutr.*, 1993, **123**, 269–274.

14 C. Ruckenstuhl, C. Netzberger, I. Entfellner, D. Carmona-Gutierrez, T. Kickenweiz, S. Stekovic, C. Gleixner, C. Schmid, L. Klug, A. G. Sorgo, T. Eisenberg, S. Buttner, G. Marino, R. Koziel, P. Jansen-Durr, K. U. Frohlich, G. Kroemer and F. Madeo, Lifespan extension by methionine restriction requires autophagy-dependent vacuolar acidification, *PLoS Genet.*, 2014, **10**, e1004347.

15 L. Sun, A. A. Sadighi Akha, R. A. Miller and J. M. Harper, Life-span extension in mice by preweaning food restriction and by methionine restriction in middle age, *J. Gerontol., Ser. A*, 2009, **64**, 711–722.

16 K. Zou, S. Rouskin, K. Dervishi, M. A. McCormick, A. Sasikumar, C. Deng, Z. Chen, M. Kaeberlein, R. B. Brem, M. Polymenis, B. K. Kennedy, J. S. Weissman, J. Zheng, Q. Ouyang and H. Li, Life span extension by glucose restriction is abrogated by methionine supplementation: Cross-talk between glucose and methionine and implication of methionine as a key regulator of life span, *Sci. Adv.*, 2020, **6**, eaba1306.

17 E. Enriquez-Hesles, D. L. Smith, N. Maqani, M. B. Wierman, M. D. Sutcliffe, R. D. Fine, A. Kalita, S. M. Santos, M. J. Muehlbauer, J. R. Bain, K. A. Janes, J. L. Hartman, M. D. Hirschey and J. S. Smith, A cell-nonautonomous mechanism

of yeast chronological aging regulated by caloric restriction and one-carbon metabolism, *J. Biol. Chem.*, 2021, **296**, 100125.

18 A. Annibal, R. G. Tharyan, M. F. Schonewolff, H. Tam, C. Latza, M. M. K. Auler, S. Grönke, L. Partridge and A. Antebi, Regulation of the one carbon folate cycle as a shared metabolic signature of longevity, *Nat. Commun.*, 2021, **12**, 3486.

19 J. W. Williams, J. F. Morrison and R. G. Duggleby, Methotrexate, a high-affinity pseudosubstrate of dihydrofolate reductase, *Biochemistry*, 1979, **18**, 2567–2573.

20 H. M. Blank, S. E. Hammer, L. Boatright, C. Roberts, K. E. Heyden, A. Nagarajan, M. Tsuchiya, M. Brun, C. D. Johnson, P. J. Stover, R. Sitcheran, B. K. Kennedy, L. G. Adams, M. Kaeberlein, M. S. Field, D. W. Threadgill, H. L. Andrews-Polymenis and M. Polymenis, Late-life dietary folate restriction reduces biosynthesis without compromising healthspan in mice, *Life Sci. Alliance*, 2024, **7**, e202402868.

21 D. J. Asby, F. Cuda, M. Beyaert, F. D. Houghton, F. R. Cagampang and A. Tavassoli, AMPK Activation via Modulation of De Novo Purine Biosynthesis with an Inhibitor of ATIC Homodimerization, *Chem. Biol.*, 2015, **22**, 838–848.

22 G. C. Williams, Pleiotropy, Natural-Selection, and the Evolution of Senescence, *Evolution*, 1957, **11**, 398–411.

23 M. V. Blagosklonny, Revisiting the antagonistic pleiotropy theory of aging: TOR-driven program and quasi-program, *Cell Cycle*, 2010, **9**, 3151–3156.

24 G. S. Ducker and J. D. Rabinowitz, One-Carbon Metabolism in Health and Disease, *Cell Metab.*, 2017, **25**, 27–42.

25 M. Reina-Campos, M. T. Diaz-Meco and J. Moscat, The complexity of the serine glycine one-carbon pathway in cancer, *J. Cell Biol.*, 2020, **219**(1), e201907022.

26 A. Rosenzweig, J. Blenis and A. P. Gomes, Beyond the Warburg Effect: How Do Cancer Cells Regulate One-Carbon Metabolism?, *Front. Cell Dev. Biol.*, 2018, **6**, 90.

27 C. Lopez-Otin, M. A. Blasco, L. Partridge, M. Serrano and G. Kroemer, The hallmarks of aging, *Cell*, 2013, **153**, 1194–1217.

28 A. Qiu, M. Jansen, A. Sakaris, S. H. Min, S. Chattopadhyay, E. Tsai, C. Sandoval, R. Zhao, M. H. Akabas and I. D. Goldman, Identification of an intestinal folate transporter and the molecular basis for hereditary folate malabsorption, *Cell*, 2006, **127**, 917–928.

29 M. Visentin, N. Diop-Bove, R. Zhao and I. D. Goldman, The intestinal absorption of folates, *Annu. Rev. Physiol.*, 2014, **76**, 251–274.

30 J. L. Parker, J. C. Deme, G. Kuteyi, Z. Wu, J. Huo, I. D. Goldman, R. J. Owens, P. C. Biggin, S. M. Lea and S. Newstead, Structural basis of antifolate recognition and transport by PCFT, *Nature*, 2021, **595**, 130–134.

31 S. Forli, R. Huey, M. E. Pique, M. Sanner, D. S. Goodsell and A. J. Olson, Computational protein-ligand docking and virtual drug screening with the AutoDock suite, *Nat. Protoc.*, 2016, **11**, 905–919.

32 K. Gallo, E. Kemmler, A. Goede, F. Becker, M. Dunkel, R. Preissner and P. Banerjee, SuperNatural 3.0-a database of natural products and natural product-based derivatives, *Nucleic Acids Res.*, 2023, **51**, D654–D659.

33 A. Daina, O. Michielin and V. Zoete, SwissADME: a free web tool to evaluate pharmacokinetics, drug-likeness and medicinal chemistry friendliness of small molecules, *Sci. Rep.*, 2017, **7**, 42717.

34 G. L. Sutphin and M. Kaeberlein, Measuring Caenorhabditis elegans Life Span on Solid Media, *J. Visualized Exp.*, 2009, e1152.

35 R. S. Peesapati, B. L. Austin-Byler, F. Z. Nawaz, J. B. Stevenson, S. A. Mais, R. N. Kaya, M. G. Hassan, N. Khanal, A. C. Wells, D. Ghiai, A. K. Garikapati, J. Selhub and E. T. Kipreos, A specific folate activates serotonergic neurons to control C. elegans behavior, *Nat. Commun.*, 2024, **15**, 8471.